J. Fluid Mech. (2006), *vol.* 559, *pp.* 335–353.
doi:10.1017/S0022112006000358 Printed in the United Kingdom

Nonlinear coupling of fluctuating drag and lift on cylinders undergoing forced oscillations

By B.-H. KIM† AND D. R. WILLIAMS

Fluid Dynamics Research Center, Illinois Institute of Technology, Chicago, IL 60616, USA

(Received 21 June 2005 and in revised form 30 December 2005)

Experiments with cylinders undergoing forced oscillations show a coupling between the fluctuating lift and drag forces as a result of nonlinear wave interactions. The fluctuating lift and drag components are computed from the instantaneous pressure around the azimuth of a circular cylinder measured with an array of miniature microphones. Quadratic nonlinear interaction between the von Kármán vortex-shedding modes and the forcing field produces sum and difference modes, which appear in the spectrum of the surface pressure signals when the forcing frequency is different from the von Kármán vortex-shedding frequency, f_o. The spatial symmetry of the interacting modes determines whether the combination modes appear in the lift spectrum or the drag spectrum. Furthermore, the spatial symmetry of the modes can be predicted from the symmetries of the two interacting parent modes. Crossflow excitation of the cylinder produces combination modes that appear in the drag spectrum. Consequently, attempts to enhance the fluctuating lift by crossflow excitation will necessarily affect the fluctuating drag through nonlinear interaction.

1. Introduction

The ability to predict accurately the response of a structure to unsteady excitation by a flow field has been a major challenge to engineers. Von Kármán vortex shedding behind a cylinder, as shown in figure 1, may excite resonant oscillations in a structure when there is a match between the flow and structural frequencies. Energy from the flow at specific frequencies is transferred to the body, which may lead to large-amplitude oscillations and structural failure. One example is the failure of a thermocouple well in a sodium pipe in a prototype fast breeder reactor which was described by Yamaguchi *et al.* (1997). Under certain conditions, simplifying approximations about the fluid–structure interaction can be made. For example, when there is a large difference between the vortex-shedding frequency and the structural modes, then the flow is decoupled from the structure. However, without the ability to predict when coupling will occur, the engineer cannot be certain whether the simpler approach is correct.

Many elements of the flow-induced vibration problem are illustrated by considering the forces acting on a towed cable. Long cables have several discrete structural modes. The vortex-shedding frequency usually varies along the length of the cable, because of the cable angle with respect to the flow, or end effects. Non-resonant frequencies do not contribute to the excitation, but are still important to the dynamics of the cable because they act to damp the motion. In the regions along the cable where

† Present address: Samsung Advanced Institute of Technology, Gyeonggi-do, Korea.

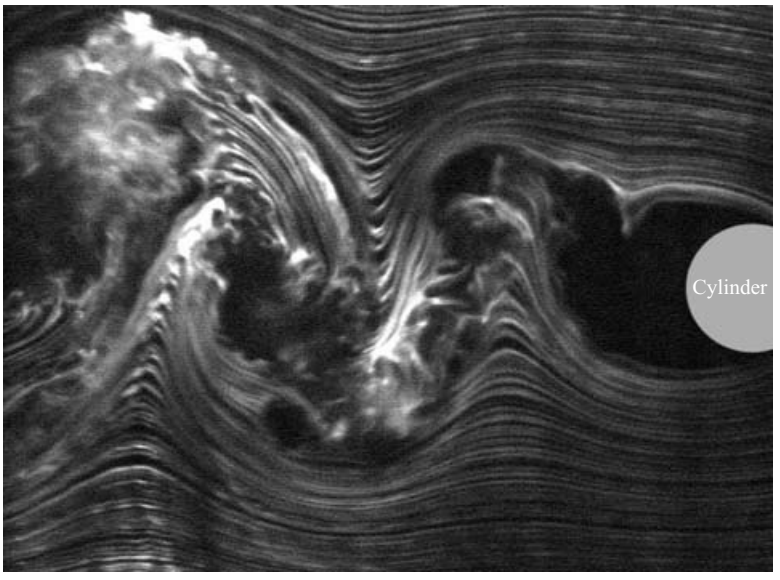

FIGURE 1. Von Kármán vortex shedding behind a cylinder ($Re = 1.52 \times 10^4$).

there is a match between the vortex-shedding frequency and one of the structural modes, the appropriate conditions exist for energy transfer from the flow to the body which can excite vibrations. The phenomenon of 'lock-in' or 'synchronization' occurs in these regions when the cable amplitude is sufficiently large. Vandiver (1993) used a Green's function approach to model structural vibrations of this type. Jong (1984) used bi-spectral techniques to investigate the coupling between crossflow and in-line motion of a long flexible cable under lock-in and non-lock-in cases. With the cross-bicoherence analysis, Jong established that a quadratic correlation existed between the crossflow and in-line responses of the flexible cable.

Flow-induced vibrations of long cylindrical structures usually have the largest amplitude in the crossflow direction. Although the fluctuating drag coefficients are normally lower and the corresponding streamwise displacements are smaller, they should not be neglected. The thermocouple failure mentioned above occurred because of in-line oscillations. It is also known (see Griffin & Ramberg 1982) that the mean drag on the body will more than double when the structure experiences flow-induced vibration and lock-in. Nevertheless, workers have tended to focus more on the mechanics of the lift forces.

Because of the importance of the lift forces, particularly in the case of modelling flow-induced vibrations, the effects of fluctuating drag are often ignored or lumped into a simplified damping model. The commonly used Hartlen & Currie-type (see Hartlen & Currie 1970) wake–oscillator models couple fluctuating lift from the wake with a structural oscillator model to determine the regions of 'lock-in'. Vandiver's approach ignores fluctuating drag, but includes the instantaneous crossflow velocity in a linear model to account for hydrodynamic damping of the cylinder motion. Olinger & Sreenivasan (1988) used a modern dynamical systems approach to model regions of lock-in based on forced crossflow oscillations, but the approach does not include fluctuating drag.

Historically, experiments were conducted in three different ways to study the interaction between the wake and the structure. The first type is 'free-oscillation'

where the cylinder is mounted on springs and the unsteady loading from the wake provides the external force. The second type is 'forced-oscillation' using a separate controllable forcing mechanism to move the cylinder. The third type introduced by Hover, Techet & Triantafyllou (1998) is a hybrid of the first two. It uses feedback from the flow to force the cylinder in response to the fluid force, which allows the effective damping and inertia of the cylinder to be independently controlled. In the latter two cases, side-to-side motion associated with fluctuating lift has been studied almost exclusively.

Here we report on experiments forcing a rigid cylinder, designed to study the nonlinear response of the wake to open-loop forcing with particular emphasis placed on the nonlinear interaction between fluctuating lift and drag. Similarly to the experiments by Jong (1984) with a flexible cable, it will be shown that a quadratic nonlinearity connects the fluctuating lift (crossflow motion) and drag (in-line motion) together. In contrast to Jong's measurements of cable acceleration, we measure the instantaneous pressure distribution around the mid-section of the cylinder to obtain the fluctuating lift and drag coefficients. It will be shown that depending on the symmetry of the forcing field, the oscillation of the structure at a particular frequency in one direction produces sum and difference modes in the orthogonal direction.

An additional motivation for this forced cylinder experiment is to establish a connection between the instantaneous surface forces and the nonlinear behaviour of the wake. In an earlier experiment by Williams, Mansy & Amato (1992), the response of a stationary cylinder wake to symmetric and antisymmetric disturbances was investigated by measuring the wake velocity profiles at $x/D = 4$ and 5. It was shown that the spatial symmetry of the combination modes formed by nonlinear interactions between the forcing field and the von Kármán vortex street followed a simple set of symmetry rules. In this paper, it will be shown that the instantaneous lift and drag forces acting on the oscillating cylinder follow the same set of rules.

2. Experimental set-up

The 'forced-oscillation' approach was used in this experiment, as a way to study the unsteady forces on the structure when the system is not in resonance. The cylinder model used was 50.8 mm diameter, D, mounted vertically in a wind tunnel (figure 2). The cylinder was 610 mm long with circular end plates placed 510 mm apart which gives an aspect ratio of 10:1. The cross-section of the wind-tunnel test section was 610 mm by 410 mm. The free-stream speed measured with a Pitot tube and micromanometer was held constant at $4.5 \pm 0.2\,\mathrm{m\,s^{-1}}$. The Reynolds number based on cylinder diameter was 1.52×10^4. The coordinate system was chosen with the origin at the centre of the cylinder, and the x-axis aligned with the flow direction. The z-axis is coincident with the cylinder axis, and the y-axis transverse to the flow. The azimuthal coordinate, defines $\theta = 0$ to be at the forward stagnation point. The von Kármán vortex-shedding frequency was 17.5 ± 0.5 Hz corresponding to a Strouhal number of 0.197.

Forcing of the cylinder motion was done with a PMI printed circuit motor connected to a Scotch-yoke mechanism. The Scotch-yoke mechanism provides a very clean sinusoidal motion, such that the spectrum of the displacement signal showed the first harmonic amplitude to be four orders of magnitude lower than the fundamental. The peak-to-peak displacement amplitude of the cylinder was measured with a dial indicator. The entire apparatus could be rotated by 90°, allowing the cylinder to move in either the crossflow or in-line direction as indicated in figure 3.

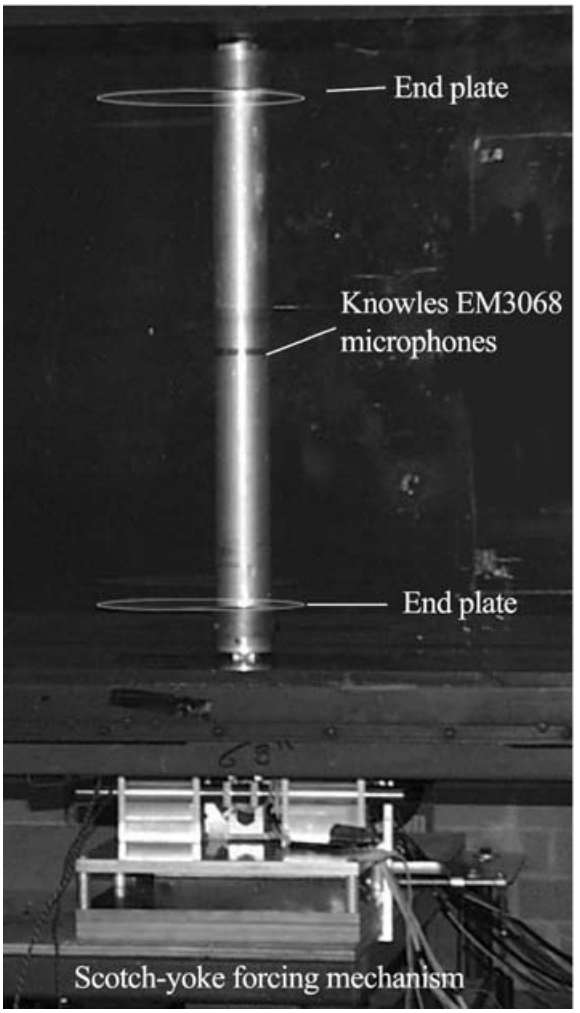

FIGURE 2. Cylinder in wind-tunnel test section showing forcing mechanism.

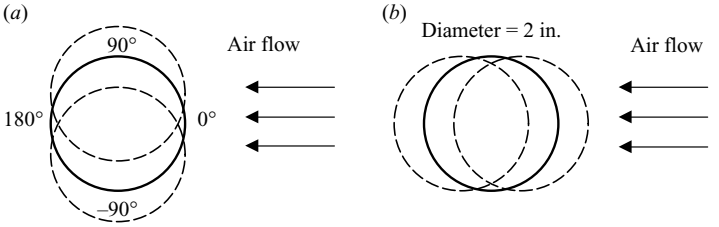

FIGURE 3. Forcing directions. (*a*) Crossflow forcing, (*b*) in-line flow forcing.

Measurements of the fluctuating surface pressure were made with 18 miniature Knowles EM-3068 microphones. The microphones were mounted inside the cylinder at its midsection. Starting at the forward stagnation point, they were spaced 20° apart around the azimuth. The data were acquired digitally with a 12 bit analogue-to-digital converter in a Pentium-based computer. Signals from the microphones were bandpass filtered between 6 Hz and 300 Hz.

The Knowles microphones were dynamically calibrated against a B&K model 4310 microphone, which in turn had been calibrated using a B&K sound level calibrator (type 4321.) An 18 Hz sound wave was produced with a loudspeaker, using sufficient amplitude to reach fluctuating pressure levels matching those in the experiment. Repeatability measurements were done by rotating the cylinder, so that the Knowles microphones in the cylinder would overlap their readings. The uncertainty in the C_p measurements was determined to be $\Delta C'_p = 0.0024$. The local C'_p values ranged from 0.02 to 0.17 giving a relative C'_p error ranging from 12 % to 1.4 %. The fluctuating lift and drag coefficients are computed as a weighted sum of the C'_p measurements, so the relative error in the C'_l and C'_d measurement is approximately 3 %.

3. Results

3.1. *Spectral analysis*

The fluctuating pressure coefficient C'_p on the surface of the cylinder is defined by $C'_p = p'/\rho U^2/2$ where p' is the root-mean-square pressure fluctuation measured by the Knowles microphones. Fluctuating lift and drag coefficients were computed using the fluctuating pressure $C'_p(t)$ from the instantaneous pressure signals taken around the cylinder. The instantaneous sectional lift and drag were computed using

$$C'_l(t) = \frac{1}{2}\sum_{i=1}^{M} C'_p(t, \theta_i)\sin(\theta_i)\Delta\theta, \tag{3.1}$$

$$C'_d(t) = \frac{1}{2}\sum_{i=1}^{M} C'_p(t, \theta_i)\cos(\theta_i)\Delta\theta, \tag{3.2}$$

where M is the maximum number of measurement points around the cylinder. These equations neglect the fluctuating viscous forces acting on the cylinder. According to Zdravkovich (1997), the viscous drag forces at $Re = 15\,200$ are negligible compared to the pressure drag and lift.

Figure 4 shows the lift and drag fluctuations under the lock-in condition with von Kármán vortex-shedding frequency of 18 Hz and Reynolds number, $Re = 1.52 \times 10^4$. The signals show that the frequency of drag fluctuations is twice that of lift fluctuations, as it is always under lock-in conditions.

The power spectra computed in this study are based on the pressure fluctuations on the cylinder surface. In order to reduce the statistical variance, the data were divided into 10 sets of $512(2^9)$ points. The frequency resolution for the spectra was 0.389 Hz with a data-sampling rate of 200 samples per second. Figures 5(*a*) and 5(*b*) show the pressure coefficient spectra distributions plotted against the azimuthal angles in crossflow and in-line forced oscillations, respectively. The dominant peaks correspond to the von Kármán vortex-shedding at $f_o = 17.5$ Hz and the forcing modes, $f_e = 14$ Hz. The von Kármán vortex-shedding mode has a maximum peak located 80° from the forward stagnation point. The maximum of the sum mode ($f_e + f_o = 32.5$ Hz) of the two primary frequencies appears near 180° in the crossflow forcing. The harmonic modes show that the nonlinear effects are significant on the cylinder surface. In the base region, the second harmonic of the vortex shedding is noticeable. These second harmonic modes contribute to the fluctuating drag forces, which have twice the frequency of the lift fluctuating forces.

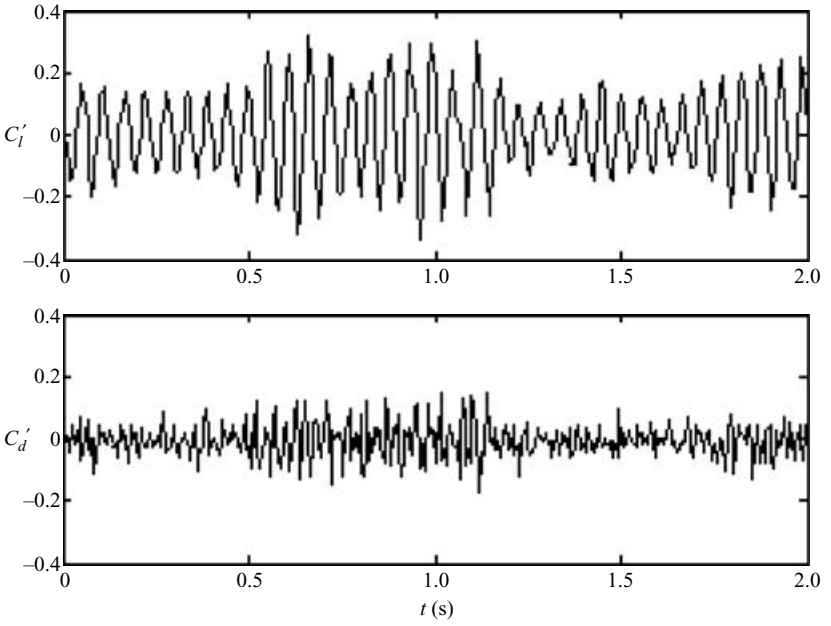

FIGURE 4. Time series of lift and drag coefficients with a stationary cylinder ($Re = 1.52 \times 10^4$).

The fluctuating pressures acting on the stationary cylinder were decomposed into the fluctuating lift and drag time series by equations (3.1) and (3.2). Figures 6(a) and 6(b) show C_l' and C_d' spectra with the stationary cylinder, respectively. The von Kármán vortex-shedding mode f_o at 18 Hz and its second harmonic $3f_o$ at 54 Hz appear in the lift coefficient spectrum, while the first harmonic mode, $2f_o$ is seen at 36 Hz in the drag coefficient spectrum. The fluctuating lift coefficient spectrum shows that the majority of the energy remains at the vortex-shedding mode at f_o, while the first harmonic of the vortex shedding at $2f_o$ is dominant in the drag spectrum for the stationary cylinder case. It is obvious that the antisymmetric Karman vortex-shedding mode appears in the lift spectrum. The peaks at 22 Hz, 39 Hz and 82 Hz in the spectra are wind-tunnel resonance frequencies. However, because there is no phase coherence between these tunnel modes and the wake modes, i.e. no bicoherence peaks, then there is no significant interaction between the tunnel modes and the wake modes.

Figure 7 shows the lift and drag coefficient spectra for the crossflow forced case with forcing frequency of 14 Hz. The forcing and von Kármán vortex-shedding modes are peaks at $f_e = 14$ Hz and $f_o = 17.5$ Hz in the lift spectrum, respectively. The first harmonic of the von Kármán vortex-shedding mode, $2f_o$ appears at 35 Hz in both the lift and drag spectra. In the drag coefficient spectrum, the first harmonic $2f_o$ of the von Kármán vortex frequency and the sum mode $f_o + f_e$ at 31.5 Hz appear as dominant peaks in figure 7(b). Note that the combination modes appear in the drag coefficient spectrum only when the forcing is in the crossflow direction.

When the cylinder is forced to oscillate in the in-line direction, combination modes appear in both the lift and drag spectra. Figure 8(a) shows the lift coefficient spectrum with the $f_o \pm f_e$ combination modes. The difference mode appears at 3.5 Hz and the sum mode at 31.5 Hz. The in-line forcing produces disturbances that are spatially symmetric about the wake centreline and on the surface of the cylinder; therefore, the

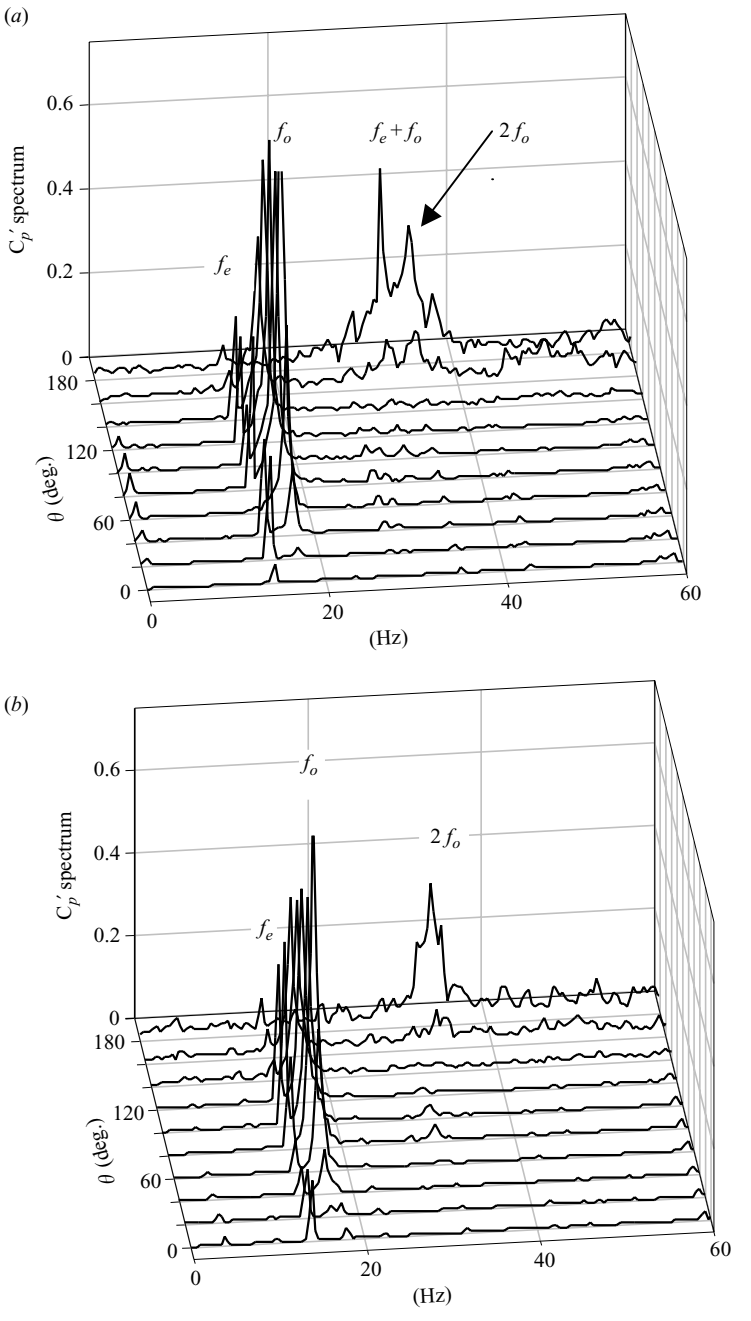

FIGURE 5. C_p' spectra along the azimuthal angles, (*a*) crossflow forcing ($\alpha = 0.07$) and (*b*) inline forcing ($\alpha = 0.07$).

peak for symmetric forcing mode can be seen in the drag spectrum with the frequency of 14 Hz.

To detect evidence of the quadratic nonlinear coupling between the drag and lift acting on the forced cylinder, higher orders of spectral techniques based on the Fourier transform such as the cross-bispectrum and cross-bicoherence are introduced (Kim &

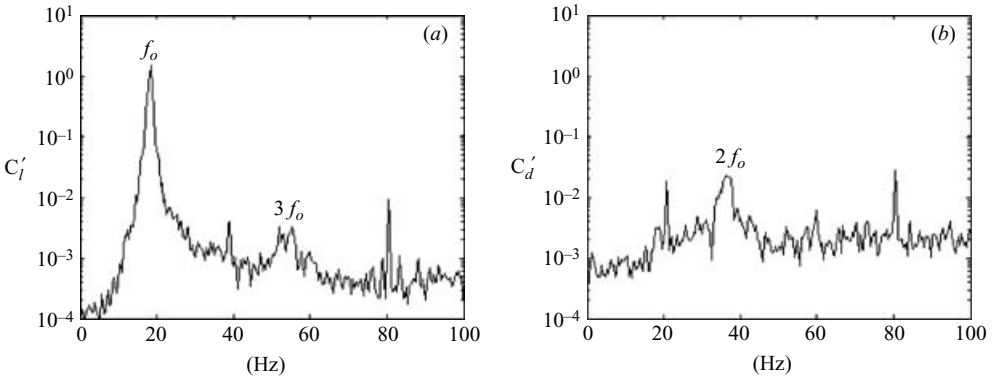

FIGURE 6. Stationary cylinder (*a*) C_l' spectrum and (*b*) C_d' spectrum.

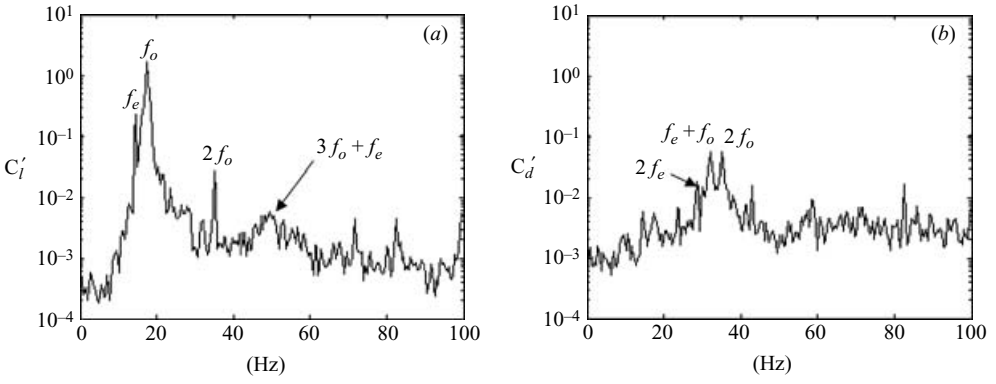

FIGURE 7. Lift and drag spectra with crossflow forcing of the cylinder at 14 Hz, and $\alpha = 0.07$ (*a*) C_l' spectrum and (*b*) C_d' spectrum.

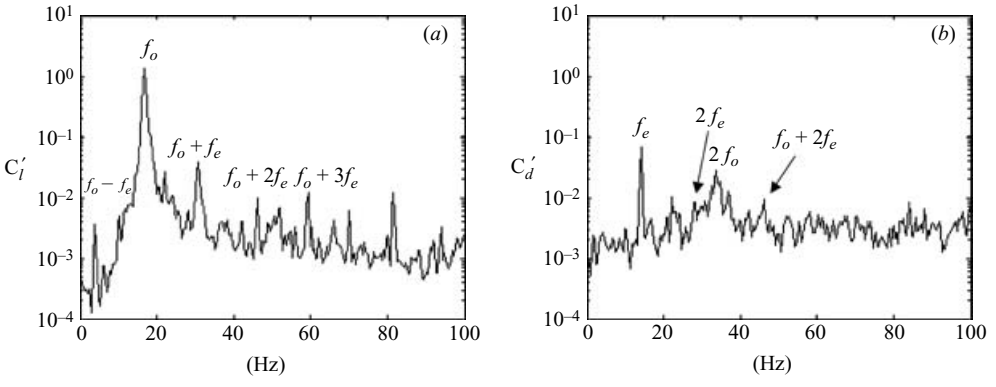

FIGURE 8. Lift and drag spectra with inline forcing at a frequency of 14 Hz, and $\alpha = 0.07$ (*a*) C_l' spectrum and (*b*) C_d' spectrum.

Powers 1979). The cross-bispectrum in equation (3.3) and cross-bicoherence in equation (3.4) can be expressed as:

$$B_{xxy}(f_i, f_j) = \lim_{T\to\infty} \frac{1}{T} E[X^*(f_i)X^*(f_j)Y(f_i + f_j)], \tag{3.3}$$

$$b_c^2(f_i, f_j) = \frac{|B_{xxy}(f_i f_j)|^2}{E[|X(f_i)X(f_j)|^2]E[|Y(f_i + f_j)|^2]}, \tag{3.4}$$

where $X(f) = FFT(x(t))$, $Y(f) = FFT(y(t))$ and $E[\ldots]$ denotes a time average, where X^* is the complex conjugate of X.

In nonlinear systems, frequency components can interact with one another to form new components at their sum and difference frequencies, commonly referred to as combination modes. The phases of the combination modes are related to the phases of the primary interacting 'parent' modes. The preservation of the phase information in the bispectrum is an important property, which is useful for investigating nonlinear quadratic coupling. If the three modes $X(f_i)$, $X(f_j)$ and $Y(f_i + f_j)$ are uncorrelated, they will have independent random phases, and the bispectrum will result in a near-zero value through the statistical averaging process. On the other hand, when the three modes are correlated the bicoherence will approach unity.

When computing the cross-bicoherence with two sets of time series data $x(t)$ and $y(t)$, one should be note that $y(t)$ is the signal containing the resultant sum and difference modes from the primary modes in $x(t)$. In figure 9, the cross-bicoherence of $x(t) = C_l'(t)$, and $y(t) = C_d'(t)$ corresponding to the spectra shown in figures 6, 7 and 8 demonstrates that the lift and drag forces are coupled. The coupling between lift and drag is obvious for the stationary cylinder case, as seen in figure 9(*a*). The stationary cylinder shows two dominant peaks at $(f_x, f_y) = (17.5, 17.5)$ and $(-17.5, 52.5)$ with bicoherence values at approximately 0.5. The spectral peak at $2f_o(35\,\text{Hz} = 17.5(f_o) + 17.5(f_o))$ in the spectrum of C_d', shown earlier in figure 6*b*, is generated by the self-interaction of the von Kármán vortex-shedding mode (f_o). What is not so obvious is the interaction of the fundamental and second harmonic of the vortex-shedding mode ($2f_o = 3f_o(52.5\,\text{Hz}) - f_o(17.5\,\text{Hz})$), which also contributes to the harmonic.

The magnitudes of the peaks appearing in the cross-bicoherence are summarized below, along with the coupling relations between the peaks seen in the spectra of figures 6, 7 and 8.

Stationary cylinder

(*a*) $f_o(17.5\,\text{Hz}) + f_o(17.5\,\text{Hz}) \rightarrow 2f_o(35\,\text{Hz})$, $b_c^2(17.5, 17.5) = 0.74$,

(*b*) $3f_o(52.5\,\text{Hz}) - f_o(17.5\,\text{Hz}) \rightarrow 2f_o(35\,\text{Hz})$, $b_c^2(52.5, -17.5) = 0.62$.

Crossflow forcing

(*a*) $f_e(14\,\text{Hz}) + f_e(14\,\text{Hz}) \rightarrow 2f_e(28\,\text{Hz})$, $b_c^2(14, 14) = 0.54$,

(*b*) $f_o(18\,\text{Hz}) + f_o(18\,\text{Hz}) \rightarrow 2f_o(36\,\text{Hz})$, $b_c^2(18, 18) = 0.43$,

(*c*) $f_o(18\,\text{Hz}) + f_e(14\,\text{Hz}) \rightarrow f_o + f_e(32\,\text{Hz})$, $b_c^2(18, 14) = 0.63$,

(*d*) $[2f_o + f_e](50\,\text{Hz}) - f_e(14\,\text{Hz}) \rightarrow 2f_o(36\,\text{Hz})$, $b_c^2(50, -14) = 0.53$,

(*e*) $[f_o + 2f_e](46\,\text{Hz}) - f_e(14\,\text{Hz}) \rightarrow [f_o + f_e](32\,\text{Hz})$, $b_c^2(46, -14) = 0.48$.

In-line flow forcing

(*a*) $f_o(17\,\text{Hz}) + f_o(17\,\text{Hz}) \rightarrow 2f_o(34\,\text{Hz})$, $b_c^2(17, 17) = 0.48$,

(*b*) $[(f_o + f_e)](31\,\text{Hz}) - f_o(17\,\text{Hz}) \rightarrow f_e(14\,\text{Hz})$, $b_c^2(31, 14) = 0.62$,

(*c*) $[f_o + 2f_e](60\,\text{Hz}) - [f_o + 2f_e](46\,\text{Hz}) \rightarrow f_e$, $b_c^2(14\,\text{Hz})$, $b_c^2(60, 46) = 0.48$.

For the crossflow forcing cases, the peaks for the harmonics (f_e and f_o) and sum mode ($f_e + f_o$), in the drag coefficient spectrum are coupled with the vortex-shedding mode and forcing mode in the lift coefficient spectrum in figure 7. In the in-line forcing cases, the vortex-shedding mode and sum mode in the lift spectrum are coupled with $2f_o$ and f_e in the drag spectrum. When $x(t) = C_d'(t)$ and $y(t) = C_l'(t)$ are chosen for the bicoherence in the in-line forcing in figure 10, no significant coherence is detected, because the combinations of f_e, $2f_e$ and $2f_o$ modes in the drag spectrum cannot be

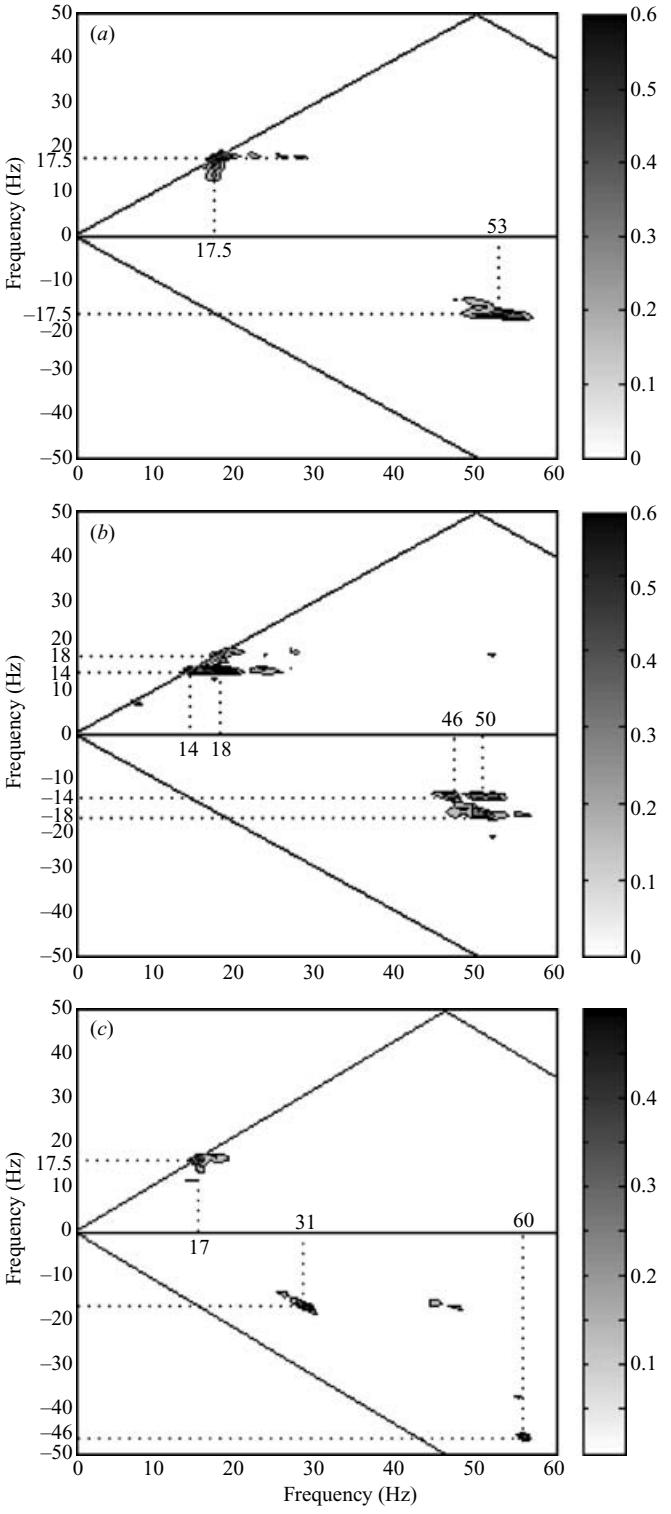

FIGURE 9. Cross-bicoherence between fluctuating lift and drag coefficients, $x(t) = C_l'$, $y(t) = C_d'$; (*a*) stationary cylinder (*b*) crossflow forcing, $f_e = 14$ Hz and $\alpha = 0.07$ and (*c*) inline-flow forcing, $f_e = 14$ Hz and $\alpha = 0.07$.

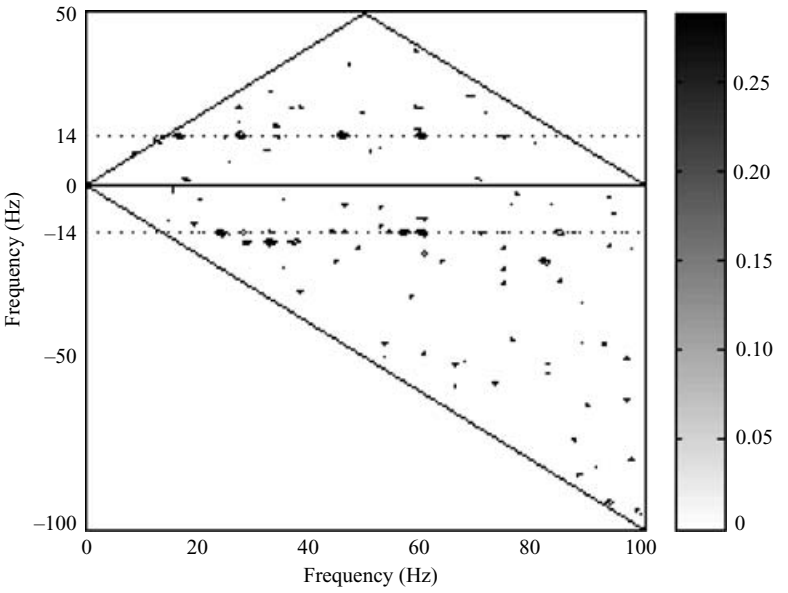

FIGURE 10. Cross-bicoherence spectrum between fluctuating lift and drag coefficients with inline-flow forcing, $x(t) = C_d'$, $y(t) = C_l'$.

coupled with f_o, $f_o + f_e$, $3f_o$, and $f_o - f_e$ modes in the lift spectrum in figure 8. It is clear from the surface pressure measurements that in cases of forced oscillations, the harmonic and combination modes play a role in the coupling between the fluctuating drag and fluctuating lift forces, which is consistent with Jong's measurements of cable oscillations.

3.2. *Decomposition into odd and even components*

Previous experiments with disturbances introduced into the boundary layer of a stationary cylinder (see Williams *et al.* 1992) determined that certain rules of symmetry were followed in quadratic nonlinear interactions in the wake. The symmetry rules are that combination modes have an even symmetry if the two parent modes are both even or both odd functions. If the parent modes have opposite symmetries, then all the combination modes are odd functions. To investigate whether the same rules are followed with oscillating cylinders, the pressure field is decomposed into even and odd functions. The technique was originally applied by Marasli, Champagne & Wygnanski (1999), who decomposed wake velocity disturbances into even and odd functions of y (crossflow direction), to determine whether the varicose mode of instability agreed with linear instability theory, as did the sinuous mode in their previous experiments. Sato (1970) also showed the velocity fluctuation of antisymmetric spectral component distributions at the fundamental mode and symmetric distributions at the first harmonic in the wake behind a flat plate. In this study, the same technique was used to decompose the pressure disturbances on the surface of the cylinder into even (symmetric) and odd (antisymmetric) components about the centreline stagnation point.

Any function can be separated into even and odd functions about a chosen centre point $\theta = 0$. The decomposition process can be applied to the pressure distribution

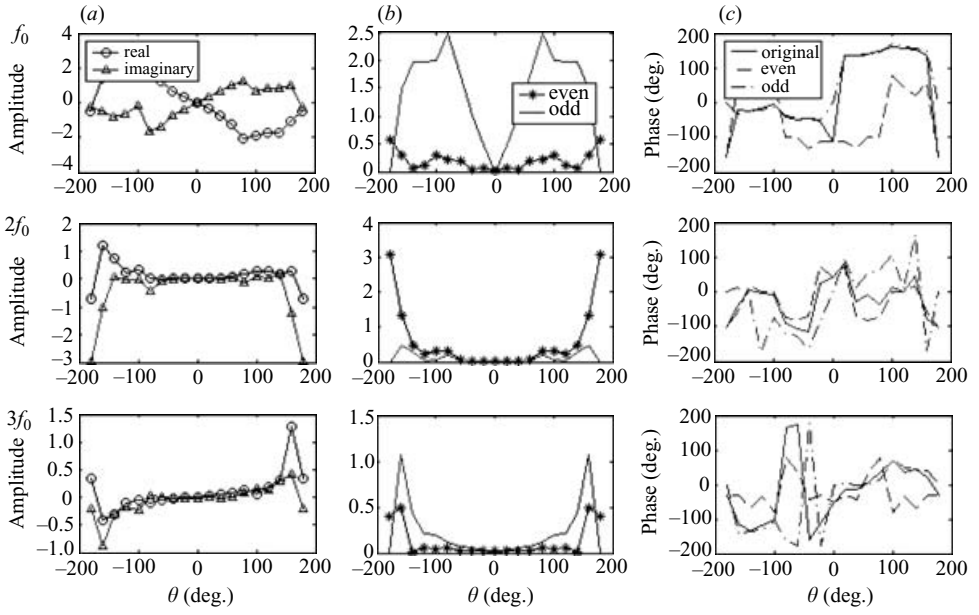

FIGURE 11. Spatial decomposition of modes with a stationary cylinder. (*a*) Real and imaginary parts, (*b*) even and odd components, (*c*) phase distributions.

occurring on the surface of the cylinder. It is defined,

$$W(f,\theta_i) = W_{even}(f,\theta_i) + W_{odd}(f,\theta_i), \tag{3.5}$$

$$W_{even} = \frac{W(f,\theta_i) + W(f,-\theta_i)}{2}, \tag{3.6}$$

$$W_{odd} = \frac{W(f,\theta_i) - W(f,-\theta_i)}{2}, \tag{3.7}$$

where $W(f,\theta_i)$ is the complex Fourier transform of the pressure coefficient, $C'_p(t,\theta_i)$. The even and odd functions are obtained by adding and subtracting $W(f,\theta_i)$ at opposing angles about the forward stagnation point as indicated in equations (3.6) and (3.7). Figures 11, 12 and 13 show the real and imaginary parts of Fourier transformed pressure coefficients, $W(f,\theta_i)$ around the cylinder at particular frequencies. The magnitude and phase distributions of the even and odd components computed using equations (3.6) and (3.7) are shown in figure 11(*b*, *c*), and figure 12(*b*, *c*).

To quantify whether a particular mode is primarily symmetric or antisymmetric, the energy in the even and odd components of each mode is obtained by integrating W_{even} and W_{odd}, around the cylinder with equations (3.8) and (3.9)

$$O(f) = \sum_{i=1}^{M} W_{odd}(f,\theta_i) W^*_{odd}(f,\theta_i)\Delta\theta, \tag{3.8}$$

$$E(f) = \sum_{i=1}^{M} W_{even}(f,\theta_i) W^*_{even}(f,\theta_i)\Delta\theta, \tag{3.9}$$

where M is the number of the pressure transducers. The ratio expresses the relative energy ratio of the odd energy against the even energy in each mode. When $O/E > 1$

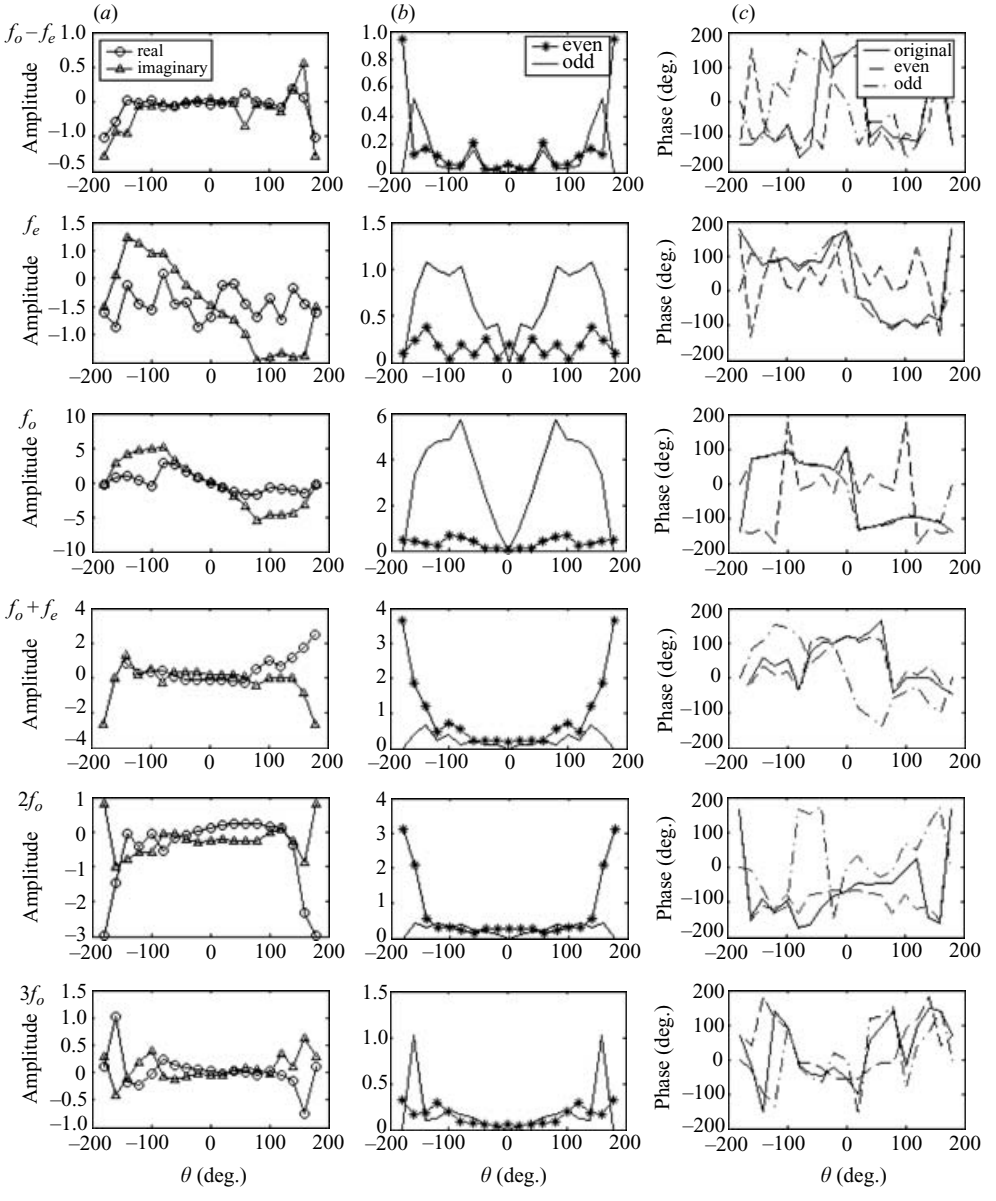

FIGURE 12. Spatial decomposition of modes with crossflow forcing, $f_o = 18$ Hz, $f_e = 14$ Hz and $\alpha = 0.07$ (*a*) Real and imaginary parts, (*b*) even and odd components, (*c*) phase distributions.

the antisymmetric component of the mode is dominant, and when $O/E < 1$ the symmetric components is dominant.

Figure 11 shows the magnitude and phase distributions with the stationary cylinder. The side-to-side oscillations of the wake at the vortex-shedding mode $f_o = 17.5$ Hz produce a dominant odd component with a 180° phase shift occurring on the wake centreline as expected for an antisymmetric mode. The relative energy ratios of $O/E = 54.9$ are given in table 1. The first harmonic $2f_o$ is symmetric (even) as indicated by $O/E = 0.05$. The first harmonic mode $2f_o$ is the result of the self-interaction of the antisymmetric (odd) vortex-shedding mode as shown in figure 9(*a*),

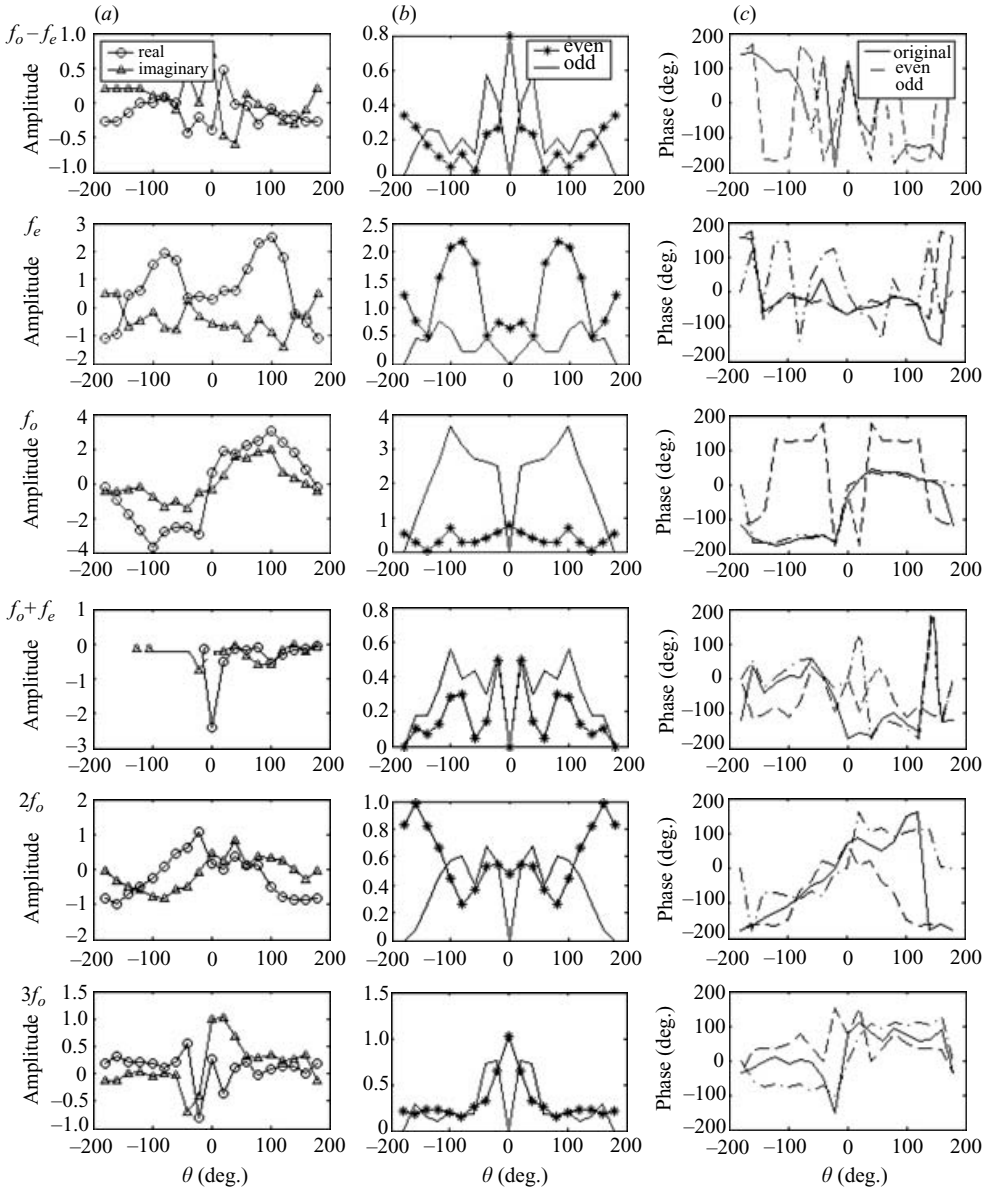

FIGURE 13. In-line-flow forcing, $f_o = 18$ Hz, $f_e = 14$ Hz and $\alpha = 0.07$. (*a*) Real and imaginary parts, (*b*) even and odd components, (*c*) phase distributions.

Mode	Stationary	Crossflow	Inline
$f_o - f_e$		0.195	1.14
f_e		14.12	0.096
f_o	54.9	96.28	32.8
$f_o + f_e$		0.072	2.29
$2f_o$	0.05	0.083	0.54
$3f_o$	4.41	4.55	0.97

TABLE 1. Energy ratio (O/E) at different modes in three cases ($\alpha = 0.07$).

so that it becomes a symmetric mode (even). The second harmonic mode $3f_o$ is antisymmetric (odd) again with $O/E = 4.41$. The second harmonic is produced by the nonlinear interaction between the antisymmetric (odd) vortex-shedding mode and the symmetric (even) first harmonic mode.

When the cylinder is forced to oscillate in either the in-line or crossflow directions, we assume the wake is being forced by predominantly symmetric or antisymmetric disturbances, respectively. Figures 12 and 13 show the decompositions of the most substantial modes with crossflow and in-line forcing; namely, the difference mode $f_o - f_e$ (4.5 Hz), the forcing mode f_e (14.7 Hz), the von Kármán vortex-shedding mode f_o (18 Hz), the sum frequency mode $f_o + f_e$ (32 Hz), the first harmonic, $2f_o$ (36 Hz) and the second harmonic $3f_o$ (54 Hz). In the crossflow forcing case, the difference mode $(f_o - f_e)$ with $O/E = 0.195$ is a symmetric mode. The sum mode $(f_o + f_e)$ is also symmetric with an energy ratio of $O/E = 0.072$ (table 1). For the sum mode shown in figure 12(*b*), the amplitude of the even function is clearly higher than the corresponding odd functions. The observation that both combination modes resulting from the crossflow forced oscillations are symmetric is consistent with the symmetry rules described above.

On the other hand, when the forced oscillations are in the in-line direction, then the symmetry rules predict that the combination modes will be antisymmetric. The data in figure 13 show that magnitudes of odd components are slightly larger than the even components, and the difference mode $(f_o - f_e)$ and the sum mode $(f_o + f_e)$ have the energy ratio of $O/E = 1.14$ and 2.28, respectively.

Antisymmetric (crossflow) forcing contributes energy to the odd components in the von Kármán vortex mode. Figure 12(*b*) shows the majority of the energy remains in the vortex-shedding mode. However, with the in-line forced oscillations at 14 Hz, the vortex-shedding mode has the energy ratio $O/E = 32.8$ which is even lower than that with the stationary cylinder. Increasing the symmetric forcing amplitudes reduces the energy of the von Kármán vortex-shedding mode.

4. Discussion

4.1. *Spatial symmetry properties in the wake*

Williams *et al.* (1992) investigated the spatial symmetry of interacting modes by observing the wake response to either symmetric or antisymmetric disturbances in the boundary layer of the circular cylinder. In their experiment, it was shown that the symmetry of the combination modes follows two fundamental rules described earlier. If the cylinder is forced in the crossflow direction, then the difference and the sum modes will be symmetric, because the antisymmetric vortex-shedding mode and antisymmetric forcing mode produced symmetric combination modes. If the forcing is in the streamwise direction, then the combination modes will be antisymmetric, since the antisymmetric vortex-shedding mode interacts with the symmetric forcing mode and produces the antisymmetric difference and sum modes. Therefore, the crossflow forced oscillations affect not only the lift force, but also the fluctuating drag forces through the increased energy in the combination modes. Similarly, the symmetric forcing can affect the fluctuating lift forces as well as the fluctuating drag forces. By the symmetry relations, we can predict the directions in which the first harmonic mode $(2f_o)$ and the second harmonic $(3f_o)$ will channel energy.

A special case occurs when the cylinder is forced at the von Kármán shedding frequency. Figure 14 shows the lift and drag coefficient spectra and their corresponding cross-bicoherence when the cylinder is forced at the von Kármán vortex-shedding

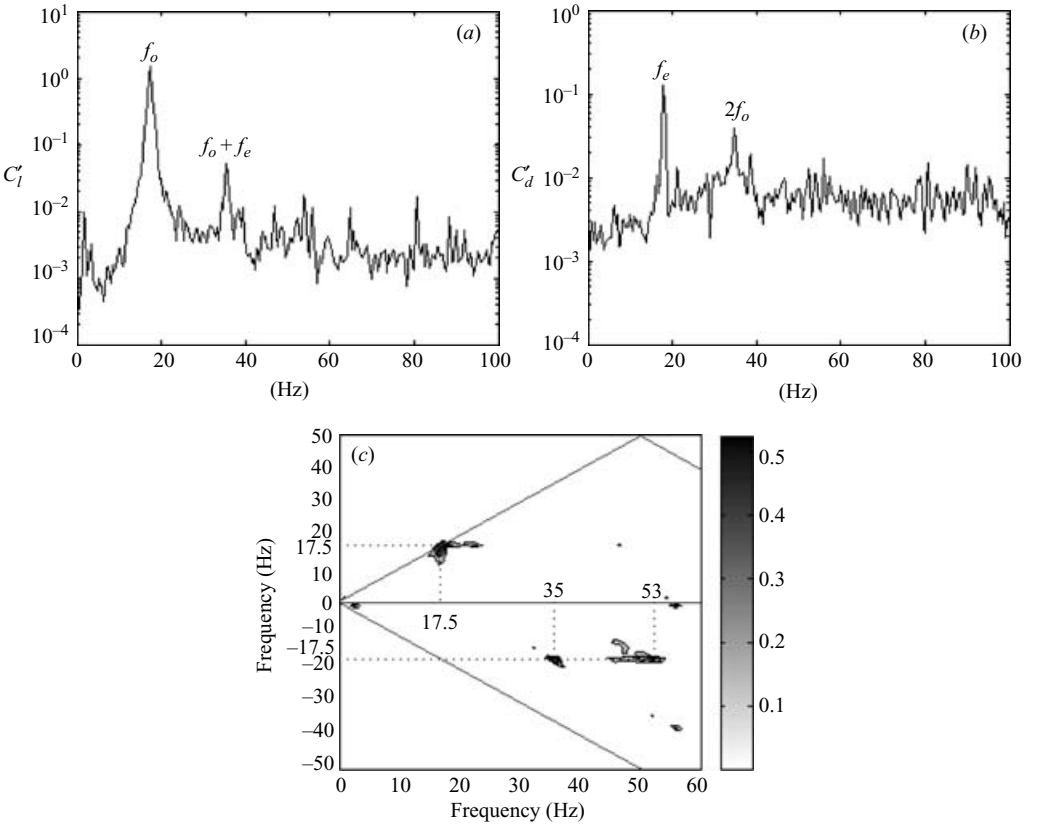

FIGURE 14. Lift and drag spectra and bicoherence with inline-flow forcing $f_o = f_e = 18$ Hz and $\alpha = 0.07$, (*a*) C_l' spectrum (*b*) C_d' spectrum and (*c*) cross-bicoherence ($x(t) = C_l'$, $y(t) = C_d'$).

frequency. The spectra in figure 14 show that in-line forced oscillations at the frequency of 18 Hz ($f_e = f_o$), produce a strong first harmonic mode $2f_o$ in both the lift and drag spectra simultaneously. The $2f_o$ mode can be both antisymmetric and symmetric by the symmetry rules. The self-interaction of the vortex-shedding mode at 18 Hz produces the symmetric $2f_o$ mode in the C_d' spectrum, while the sum mode ($f_e + f_o$) in the C_l' spectrum in figure 14(*a*) will be antisymmetric since it is the result of the interaction between the antisymmetric vortex-shedding mode (f_o) and the symmetric forcing mode (f_e). The peak at (36 Hz, −18 Hz) in the cross-bicoherence proves that the peak at 18 Hz and 36 Hz in C_l' are indeed coupled.

4.2. *Energy transfer between the forced cylinder and the fluid*

The energy transferred between the forced cylinder and the fluid is discussed in this section along with the measurements of the spectral magnitudes of parent modes and combination modes in both crossflow and in-line forced oscillations. To reduce the uncertainty of the magnitude measurements in the spectra, the magnitudes of two adjacent peaks (0.4 Hz) are averaged to obtain the magnitude at the particular frequency. The forcing amplitudes were increased gradually to provide the increasing forcing energy to the cylinder, while the forcing frequency was kept constant at $f_e = 14$ Hz. The magnitudes of C_l' and C_d' spectra in increments of forcing amplitudes are shown in figures 15 and 16 for crossflow and in-line forcing, respectively.

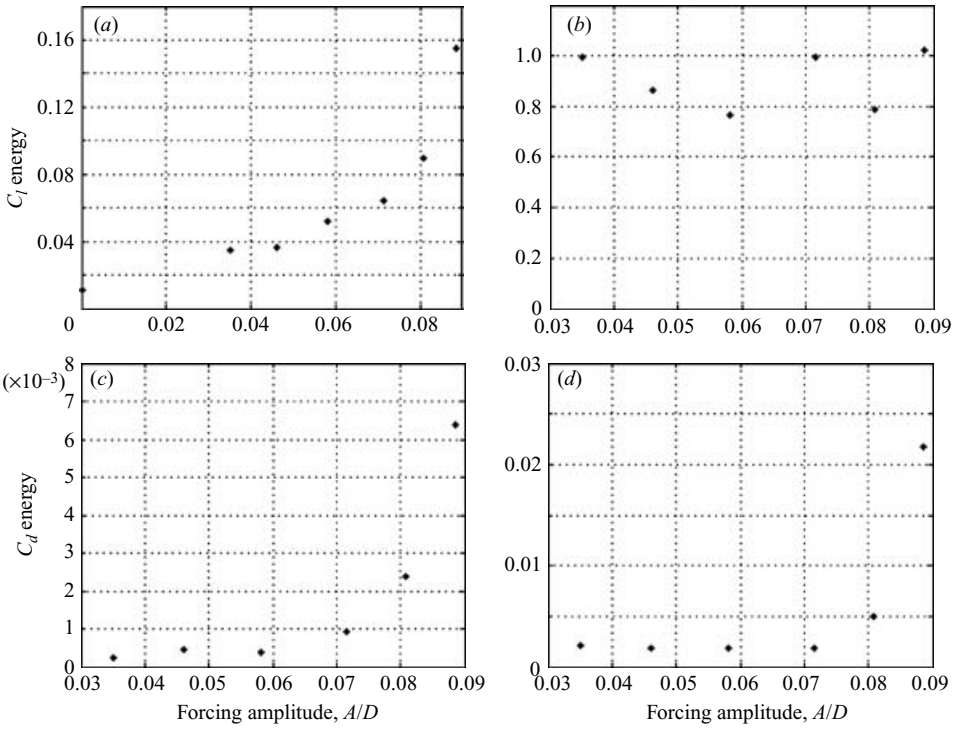

FIGURE 15. Modal energy dependence on forcing amplitude with crossflow forcing $f_o = 18$ Hz, $f_e = 14$ Hz and $\alpha = 0.07$, (*a*) f_e, (*b*) f_o, (*c*) $f_o - f_e$ and (*d*) $f_o + f_e$.

As the peak-to-peak crossflow forcing amplitude increases, the spectral magnitudes of the forcing mode increase as shown in figure 15(*a*). The spectral magnitudes of the von Kármán vortex-shedding modes do not change much, and initially decrease at low forcing amplitudes (figure 15*b*). According to the symmetry rules of the mode interaction, the spectral magnitudes of the combination modes measured in drag spectra are coupled with the forcing and vortex-shedding modes when the cylinder is undergoing crossflow oscillations. Although mode coupling does not guarantee an energy transfer to the combination modes, the data in figure 15(*c*, *d*) show a trend of increasing energy in both the difference mode and the sum mode with increasing forcing amplitudes.

When the cylinder is forced in the in-line direction with increasing forcing amplitudes, the results of the spectral magnitude measurements are similar to the cross-forcing case except for the directionality, as shown in figure 16. The forcing energy in drag increases as forcing amplitudes increase. The vortex-shedding modes are saturated in energy of approximately $O/E = 0.7$, which is less than the energy of $O/E = 0.9$ in the crossflow forcing case. The combination modes in the lift direction in figure 16(*c*, *d*) show an increase in energy from the forced oscillations, particularly in the sum mode.

In summary, the von Kármán vortex-shedding mode is not strongly affected by the forcing at the levels used in this experiment. The difference and sum modes absorb the energy from the forcing in both cases. The difference mode and the sum mode in the crossflow forcing absorb energy in the in-line direction, while in the in-line

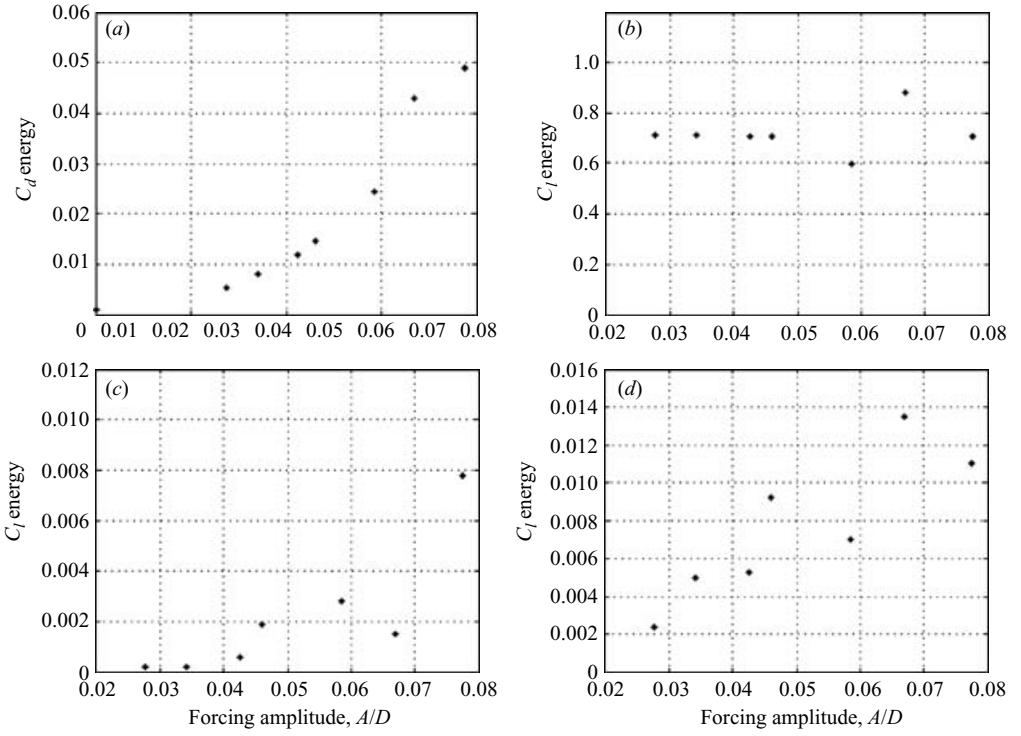

FIGURE 16. Modal energy dependence on forcing amplitude with in-line flow forcing, $f_o = 18$ Hz, $f_e = 14$ Hz and $\alpha = 0.07$, (*a*) f_e, (*b*) f_o, (*c*) $f_o - f_e$ and (*d*) $f_o + f_e$.

forcing the difference and sum modes absorb energy in the crossflow direction. These results also show the coupling between the fluctuating drag and lift forces.

5. Conclusion

Surface pressure fluctuations around a cylinder have been investigated when the cylinder is undergoing forced oscillations in crossflow and in-line directions. They show that the coupling between the fluctuating lift and drag forces exists, which is consistent with the observations of Jong. Using bi-coherence spectra, the quadratic nonlinear interactions between the von Kármán vortex-shedding modes and the forcing modes were clearly observed. The sum and difference modes generated by the parent modes play an important role in channelling energy into in-line and crossflow directions.

The decomposition of the wake pressure fluctuations on the surface of the cylinder into even and odd components has been performed. Furthermore, the combination modes were predicted by two simple symmetry rules. An antisymmetric mode interacting with a symmetric mode produces an antisymmetric mode, and the interaction between either two antisymmetric modes or two symmetric modes produces symmetric modes. When a cylinder is forced in the crossflow direction, the antisymmetric forcing mode and the antisymmetric von Kármán vortex-shedding mode generate the symmetric sum and difference modes which appear in the drag spectrum. When the cylinder is forced in the in-line direction, the antisymmetric

von Kármán vortex-shedding mode and the symmetric forcing mode generate the combination modes appearing in a lift spectrum, which is antisymmetric.

A strong second harmonic ($3f_o$) mode is observed in the fluctuating lift spectrum when the cylinder is forced at the vortex-shedding frequency in the crossflow direction. This is because antisymmetric $3f_o$ modes are generated by the interaction between the antisymmetric forcing mode and the symmetric $2f_o$ mode. For cases of in-line forcing, the first harmonic and the second harmonic mode can be antisymmetric and symmetric simultaneously, thereby appearing in both the lift and drag spectra. Their symmetric component is the result of the self-interaction of the antisymmetric fundamental (f_o) mode, or the first harmonic mode of the forcing mode ($2f_e$). The antisymmetric component is the result of the interaction between the antisymmetric fundamental (f_o) mode and symmetric forcing mode (f_e).

The spectral magnitudes have been measured in each mode with increasing forcing amplitudes to see how the energy is distributed to the combination modes. The von Kármán vortex-shedding modes are essentially saturated in energy, while other modes absorbed the energy from the forced oscillations. The difference and the sum modes in the crossflow forced oscillations absorbed energy in the drag component, while they absorbed energy in the lift component with the in-line forcing.

Support for this project by the Office of Naval Research under Grant N00014-94-0538 monitored by Dr Tom Swean is gratefully acknowledged.

REFERENCES

Griffin, O. M. & Ramberg, S. E. 1982 Some recent studies of vortex shedding with application to marine tubulars and risers. *Trans. ASME* **106**, 2–13.

Hartlen, R. T. & Currie, J. G. 1970 Lift oscillator model of vortex-induced vibration. *J. Engng Mech. Div. ASCE* **96**, 577–591.

Hover, F. S., Techet, A. H. & Triantafyllou, M. S. 1998 Forces on oscillating uniform and tapered cylinders in crossflow. *J. Fluid Mech.* **363**, 97–114.

Jong, J.-Y. 1984 The quadratic correlation between in-line and corss-flow, vortex-induced vibration of long flexible cylinders. PhD thesis, Massachusetts Institute of Technology, Cambridge.

Kim, Y. & Powers, E. 1979 Digital bispectral analysis and its applications to nonlinear wave interactions. *IEEE Trans. Plasma Sci.* **7**, 120–130.

Marasli, B., Champagne, F. & Wygnanski, I. J. 1999 Modal decomposition of velocity signals in a plane turbulent wake. *J. Fluid Mech.* **198**, 255–273.

Olinger, D. J. & Sreenivasan, K. R. 1988 Nonlinear dynamics of the wake of an oscillating cylinder. *Phys. Rev. Lett.* **60**, 797–800.

Sato, H. 1970 An experimental study of non-linear interaction of velocity fluctuations in the transition region of a two-dimensional wake. *J. Fluid Mech.* **44**, 741–765.

Vandiver, J. K. 1993 Dimensionless parameters important to the prediction of vortex-induced vibration of long, flexible cylinders in ocean currents. *J. Fluids Struct.* **7**, 423–455.

Williams, D. R., Mansy, H. & Amato, C. 1992 The response and symmetry properties of a cylinder wake subjected to localized surface excitation. *J. Fluid Mech.* **234**, 71–96.

Yamaguchi, A., Morishita, M., Wada, Y., Iwata, K. & Ichimiya, M. 1997 Failure mechanism of a thermocouple well caused by flow-induced vibration. *AD-Vol.53-1 Fluid Structure Interaction, ASME* **1**, 139–148.

Zdravkovich, M. M. 1997 *Flow Around Circular Cylinders*. Oxford University Press.